https://doi.org/10.48048/tis.2023.4350

The Effect of Different Synthesis with Chemical and Biological Methods on Properties of Silver Oxide Nanoparticles

Kiki Maesaroh[1], Muhamad Diki Permana[1,2,3], Diana Rakhmawaty Eddy[1,*] and Iman Rahayu[1]

[1]Department of Chemistry, Faculty Mathematics and Natural Sciences, Universitas Padjadjaran Sumedang, West Java 45363, Indonesia
[2]Integrated Graduate School of Medicine, Engineering and Agricultural Sciences, University of Yamanashi, Kofu 4008511, Japan
[3]Center for Crystal Science and Technology, University of Yamanashi, Kofu, Yamanashi 4008511, Japan

([*]Corresponding author's e-mail: diana.rahmawati@unpad.ac.id)

Received: 23 May 2022, Revised: 23 June 2022, Accepted: 30 June 2022, Published: 16 January 2023

Abstract

Silver oxide (Ag_2O) nanoparticles have been successfully synthesized through several methods, namely sol-gel, sonochemical, and biological methods. X-ray diffraction studies revealed that the sonochemical method produces silver oxide with high phase purity, then the sol-gel method produces another phase, namely silver crystals, while the biological method produces Ag_3PO_4 phase from the precursor media. The research showed that the sol-gel method had the smallest crystallite and particle sizes of 9.5 and 232.7 nm, respectively, compared to sonochemical and biological methods. It is known that the specific surface area of the sol-gel method has the largest value, namely 60.09 m^2/g, compared to the sonochemical and biosynthetic methods, which are 51.78 and 24.77 m^2/g, respectively. Scanning electron microscopy study showed homogeneous spherical nanoparticles of silver oxide in the sol-gel and sonochemical methods, however, the biological method resulted in the formation of non-spherical silver oxide nanoparticles in the form like flakes.

Keywords: Nanoparticles, Silver oxide, Size distribution, X-ray diffraction, Morphology

Introduction

Nanotechnology has explored opportunities to create new materials that are nano-sized and have unique chemical and physical properties that differ from their original state [1-3]. These unique properties depend on the composition, structure, shape, and size of the nanoparticles [4-6]. Nanostructures or finely dispersed nanoparticles are used in many applications such as drugs and medications [7], manufacturing and materials, environment, electronics, energy harvesting, and mechanical industry [8,9].

In recent years, nano-sized metal oxides have shown unique chemical properties including optical, magnetic, electrical, and catalytic properties, as well as a significant increase in physical properties such as mechanical hardness and thermal stability depending on the shape and size of the particles [10,11]. Silver oxide (Ag_2O) is a semiconductor material that has high chemical stability and is non-toxic [12]. Silver oxide nanoparticles have wide applications in the fields of fuel cells [13,14], photovoltaic cells [15], adsorption and photocatalysis [16,17], sensors [18], optical data storage [19], and antibacterial [20].

Various methods of silver oxide synthesis have been carried out, including chemical methods such as sol-gel synthesis [21,22], sonochemistry [23,24], solvothermal [25], and microemulsion methods [26,27], and biological methods [28,29]. These methods have been applied to produce silver oxide in various properties such as composition, crystallinity, structure, morphology, and size [30,31]. The synthesis of nanoparticles with a bottom-up approach must be able to overcome the occurrence of agglomeration and maintain the size distribution.

The sol-gel method has advantages because it can produce high-purity products, lower the synthesis temperature, and produce sizes with high homogeneity [32]. Then, sonochemical synthesis methods have been extensively studied to produce nanomaterials with unique morphology [33]. Previous studies reported that dendritic, spherical, and rod-shaped nanoparticles were successfully synthesized using ultrasonic irradiation [34]. In addition, in the synthesis of nanoparticles, efficiency in the use of materials and energy must be considered. The biological method is an environmentally friendly application of green chemistry and has received attention because it produces nanoparticles with diverse properties [35].

In this study, we study a comparison of several chemical synthesis methods, namely sol-gel and sonochemistry as well as biological methods to determine the properties of the silver oxide nanoparticles. The synthesized silver oxide nanoparticles were characterized using X-ray diffraction (XRD), scanning electron microscopy-energy dispersive spectroscopy (SEM-EDS), and particle size analyzer (PSA).

Materials and methods

Materials

The materials used in this study were distilled water, polyethylene glycol 6,000 (PEG, Sigma Aldrich), silver nitrate ($AgNO_3$, Sigma Aldrich), ethanol (C_2H_5OH, 96 %, Merck), sodium hydroxide (NaOH, 99 %, Merck), Saccharomyces cerevisiae A18, bacteriological peptone (LP0037, Oxoid), ammonium sulphate ($(NH_4)_2SO_4$, Merck), D-glucose ($C_6H_{12}O_6$, Merck), potassium dihydrogen phosphate (KH_2PO_4, Merck), and yeast extract (LP0021, Oxoid). All ingredients were used without prior treatment.

Preparation Ag_2O using chemical sol-gel method

The method used in this synthesis is the method of Yong *et al*. [36] modified. A total of 20 g of PEG was dissolved in 950 mL of distilled water until the solution was homogeneous. Then, added 0.5 g of $AgNO_3$ which has been dissolved in 50 mL of distilled water. Then, 0.5 mol/L NaOH was added dropwise to a pH of 9.8. Thereafter, the solution was stirred for 1 h at 50 °C. Then the precipitate was separated by centrifugation, washed with distilled water and ethanol, and dried at 50 °C for 24 h. The synthesized Ag_2O for sol-gel method was named AgNP-Sol.

Preparation Ag_2O using chemical sonochemical method

A total of 45 mL of 0.1 mol/L $AgNO_3$ was placed in ultrasonic (GB0102, 40 kHz 60W). Then, added 0.1 mol/L NaOH dropwise as much as 45 mL. Then, the solution was sonicated for 2.5 h [37]. The precipitate formed was then centrifuged, washed with distilled water and ethanol, and dried at 50 °C for 24 h. The synthesized Ag_2O for sonochemical method was named AgNP-Son.

Preparation Ag_2O using biological method

Yeast culture of *Saccharomyces cerevisiae* was prepared on yeast extract peptone dextrose (YEPD) media, with yeast extract (0.5 %), bacteriological peptone (0.5 %), ammonium sulphate (0.3 %), potassium dihydrogen phosphate (0.3 %), and D-glucose (20 %) which have been sterilized by autoclave. The cultures were inoculated in sterile YEPD media and incubated at room temperature with shaking at 180 rpm for 24 h, then centrifuged and the supernatant was collected.

The supernatant obtained was taken as much as 48 mL, then added with 32 mL of sterile distilled water and 8 mL of 0.2 mol/L $AgNO_3$. The mixture was then stirred at 180 rpm for 24 h. The resulting precipitate was then centrifuged at 10.000 rpm for 15 min. The precipitate formed was then centrifuged, washed with distilled water and ethanol, and dried at 100 °C for 3 h. The synthesized Ag_2O for biosynthesis method was named AgNP-Bio.

Materials characterization

The crystalline phase of the synthesized samples was identified using X-ray diffraction (XRD, Rigaku/MiniFlex 600, Tokyo, Japan) measured at room temperature using Cu Kα radiation ($\lambda = 1.5418$) with scans performed in the range of $2\theta = 20 - 80$ °. Then, to determine the surface morphology and atomic composition, the samples were analyzed using scanning electron microscopy-energy dispersive X-ray spectrometry analysis (SEM-EDS, Hitachi SU-3,500, Tokyo, Japan) with a voltage of 5.00 kV at a magnification of 5,000x. Finally, particle size was determined using a particle-size analyzer (PSA, Horiba SZ-100, Kyoto, Japan).

Results and discussion

XRD analysis

The phase structure of the sample was observed from the XRD pattern shown in **Figure 1**. The XRD pattern was compared with the Inorganic Crystal Structure Database (ICSD) 98-028-1041 for Ag_2O crystals which had a cubic structure with a space group *Pn*-3*m* [38], Ag crystals were compared with ICSD 98-018-0878 which has a cubic structure with a space group of *Fm*-3*m* [39], and Ag_3PO_4 crystals were compared with ICSD 98-020-1363 which has a cubic structure with a space group of *P*-43*n* [40]. The structure of Ag_2O has a peak at $2\theta = 32.8$ ° (111), 38.0 ° (002), 54.8 ° (022) and 65.3 ° (113), while the structure of Ag has a peak at $2\theta = 38.0$ ° (111), 44.2 ° (002), 64.3 ° (022) and 77.2 ° (113). Then, the structure of Ag_3PO_4

has a peak at 2θ = 29.5 ° (002), 33.1 ° (012), 36.4 ° (112), 47.5 ° (013), 52.4 ° (222), 56.9 ° (123), 61.3 ° (004) and 71.4 ° (124).

From **Figure 1** it can be seen that the sol-gel method is formed Ag_2O and Ag. This shows that the presence of polyethylene glycol (PEG) encourages some of the Ag^+ to be reduced to Ag^0 [41,42]. Meanwhile, in the sonochemical methods, almost all phases are formed into Ag_2O. In the biosynthetic method, there is a peak originating from Ag_3PO_4 which is probably sourced from the precursor media. The peak at 2θ = 32.8 ° indicates Ag_2O crystals with hkl planes (111), 2θ = 38.0 ° indicates Ag crystals with hkl planes (111), and 2θ = 29.5 ° indicates Ag_3PO_4 crystals with hkl planes (002) (**Figure 2**).

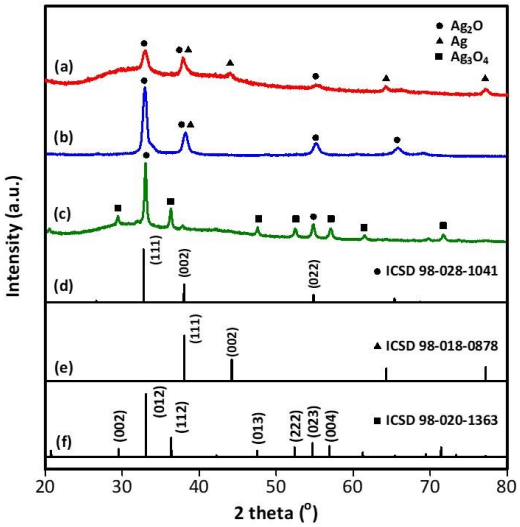

Figure 1 X-ray diffraction pattern of (a) AgNP-Sol, (b) AgNP-Son, (c) AgNP-Bio, (d) Ag_2O ICSD 98-028-1041, (e) Ag ICSD 98-018-0878, and (f) Ag_3PO_4 ICSD 98-020-1363.

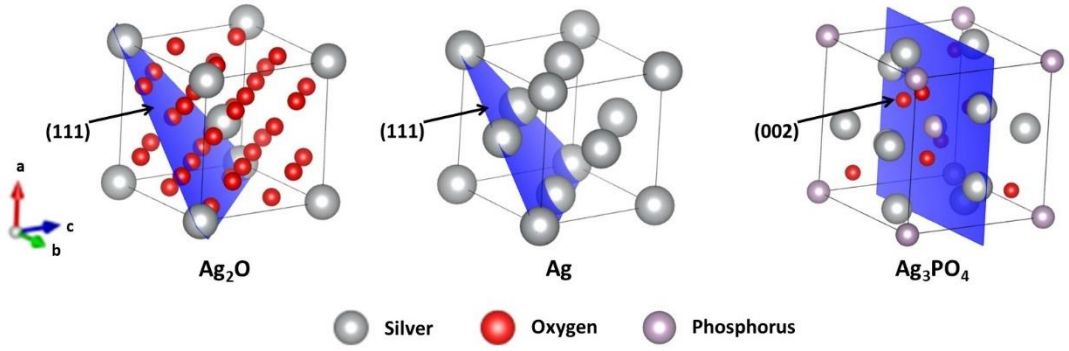

Figure 2 Crystal structure of Ag_2O and AgO with hkl planes (111), and Ag_3PO_4 with hkl planes (002).

The percentage of crystal structure was calculated using Rietveld refinement using HighScore Plus software (PANalytical 3.0.5) [43], while the coefficients of shifted polynomial functions were used to match the background. In **Table 1**, it is known that the sol-gel method with the addition of PEG produces Ag crystals, namely 13.1 %. While the biosynthetic method does not contain Ag crystals at all. Then, the goodness of fit (GoF) value is calculated to confirm the accuracy of the Rietveld refinement. GoF is a statistical model which describes how well the experimental results are obtained with a series of observations [44] and calculated using the Eq. (1).

$$GoF = (R_{wp}/R_{exp})^2 \quad (1)$$

where R_{wp} (weighted profile R-factor) is the simplest difference index and R_{exp} (expected R-factor) is the expected "best R_{wp}" quantity. **Table 1** shows that the GoF value for AgNP-Sol is the smallest, which means that the percentage calculation is accurate. On the other hand, the highest GoF value for AgNP-Son indicates low accuracy.

Table 1 Percentage of phase composition and rietveld refinement parameters of the samples.

Sample	Crystal phase (%)			Rietveld refinement parameters		
	Ag_2O	Ag	Ag_3PO_4	R_{exp}	R_{wp}	GoF
AgNP-Sol	86.90	13.10	0.00	3.45	9.77	8.03
AgNP-Son	99.80	0.20	0.00	5.08	18.18	12.81
AgNP-Bio	82.50	0.00	17.50	3.27	9.58	8.56

The unit cells of the sample are shown in **Table 2**. Ag_2O crystals synthesized by the sonochemical method have the smallest lattice volume and therefore the largest density. Based on the results of the study, the volume of AgNP-Son lattice was 104.4 $Å^3$, while in AgNP-Sol and AgNP-Bio the volume increased to 106.9 and 108.4 $Å^3$, respectively. This indicates that the biological synthetic method will produce Ag_2O crystals with low density than chemical methods.

Table 2 Crystal lattice parameters of the samples.

Sample	Ag_2O			Ag			Ag_3PO_4		
	$a=b=c$ (Å)	V ($Å^3$)	ρ (g/cm^3)	$a=b=c$ (Å)	V ($Å^3$)	ρ (g/cm^3)	$a=b=c$ (Å)	V ($Å^3$)	ρ (g/cm^3)
AgNP-Sol	4.747	106.9	7.200	4.085	68.170	10.51	-	-	-
AgNP-Son	4.709	104.4	7.370	-	-	-	-	-	-
AgNP-Bio	4.768	108.4	7.100	-	-	-	6.001	216.2	6.43

The crystallinity of the composite was calculated from the XRD pattern by comparing the crystalline and amorphous peaks. Then, the crystallite size was calculated using the Debye-Scherrer Eq. (2) of all peaks averaged [45].

$$D = (K\lambda)/(B\cos\theta) \quad (2)$$

where D is the crystallite size, K is the Scherrer constant (0.94 for cubic) [46], λ is the wavelength of X-ray radiation (Cu Kα = 0.15418 nm), B is the value of the full width at half maximum (FWHM) peak (radians), and θ is the diffraction angle (radians). Then, the strain (ε) of the lattice crystal was evaluated using Eq. (3) of (111) planes of Ag_2O crystals [47,48]. The value of this strain can be obtained from the resulting peak broadening. The strain of each sample can be different because there are different defects, such as interstitials, vacancies, dislocations, and layer fractures, which leads to different strain in the crystals.

$$\varepsilon = (B\cos\theta)/4 \quad (3)$$

Based on **Table 3**, the size of the Ag_2O crystals synthesized using the chemical method was smaller than the biological method, with the smallest being the sol-gel method. The size of the crystallites in AgNP-Sol and AgNP-Son did not differ significantly, namely 9.52 and 11.10 nm, however, the biological method has doubled in crystallite size, namely 23.18 nm. This can be understood because in the biological synthesis, the crystal formation process runs slowly and the crystals become larger. While in the sol-gel and sonochemical methods, NaOH is added and assisted by a stirring process that crystals can form quickly and make the crystallite size relatively smaller.

In contrast to the size of the crystallites, the smallest strain value was obtained by the biosynthetic Ag_2O. The strains of lattice for AgNP-Sol, AgNP-Son, and AgNP-Bio were obtained 0.00353, 0.00249, and 0.00138, respectively. Then the crystallinity of the sample is determined because the degree of crystallinity will determine the ability to flow electrons and applied for properties of electrical conductivity, dielectric constant, and photocatalysis [49,50]. It is known that the sol-gel method has the lowest crystallinity of 57.35 %, followed by biological method of 63.37 %, and the highest is the sonochemical method with crystallinity of 77.40 %.

Table 3 Crystal properties of the samples.

Sample	Crystallite size (nm)[a]			Crystal strain/ε (10^{-3})[b]	Crystallinity (%)	SSA (m^2/g)	δ (10^{15} m^{-2})
	Ag_2O	Ag	Ag_3PO_4				
AgNP-Sol	9.52 ± 0.28	14.60 ± 1.69	-	3.530	57.35	60.09	11.10
AgNP-Son	11.10 ± 1.93	-	-	2.490	77.40	51.78	8.12
AgNP-Bio	23.18 ± 1.60	-	22.16 ± 1.83	1.380	63.37	24.77	1.86

[a]using Scherrer method from average all peaks in mean ± standard deviation
[b]calculated from 2θ = 32.8 ° (111) for Ag_2O crystals

Specific surface area (SSA) is a material property of particular importance in terms of adsorption [51], heterogeneous catalysis [52], and reactions at the surface [53]. In this study, the calculated SSA is crystalline SSA with the definition as surface area (SA) of crystals per mass of crystals. SSA can be calculated by Sauter's formula (Eq. 4), where SSA is the specific surface area of Ag_2O crystals (m^2/g), D is the crystallite size of Ag_2O (m), and is the density of synthesized Ag_2O crystals (g/m^3) [54].

$$SSA = 6/(D.\rho) \quad (4)$$

The sol-gel method had the highest SSA value, followed by the sonochemical and biosynthetic methods. This SSA value is directly proportional to the size of the crystallite obtained. The SSA values from the sol-gel, sonochemical, and biosynthetic methods were 60.09, 51.78 and 24.77 m^2/g, respectively.

Dislocations are crystallographic defects, or irregularities that greatly affect many material properties in the crystal structure. The mechanism of dislocation formation is established with the help of grain boundary initiation, homogeneous nucleation, lattice and surface interfaces, precipitates, dispersed phase, or reinforcing fibers [55]. The dislocations in the sample will inhibit the movement of each other, which will then add to the greater hardness. The value of dislocations is expressed in dislocation density, where dislocation density is a measure of the number of dislocations in a unit volume of a crystalline material [56]. The dislocation density was calculated using Eq. 5, where is the dislocation density (m^{-2}) and D is the crystallite size (m) [57]. The dislocation density values of Ag_2O synthesized by sol-gel, sonochemical, and biosynthetic methods were 11.1×10^{15}, 8.12×10^{15} and 1.86×10^{15} m^{-2}, respectively. The strength of the material and the magnitude of the dislocations increase with decreasing crystallite size.

$$\delta = 1/(D^2) \quad (5)$$

SEM-EDS analysis

The morphology of particles was studied using SEM. **Figure 3** shows that the material synthesized by the chemical method has homogeneous spherical particles. However, some particle agglomeration occurs in both sol-gel and sonochemical methods. Meanwhile, biochemical methods produce particles shaped like flakes. In the sol-gel method, less agglomeration occurs compared to the sonochemical method. This shows that the sol-gel with the addition of PEG surfactant well prevents agglomeration. Generally, at the nanometer scale, metals tend to nucleate and grow into twinned particles. Ag particles are also known to have a tendency to agglomerate due to their high surface energy and high surface tension [52]. Smaller particle sizes will produce a large surface which will increase the catalytic activity of the material.

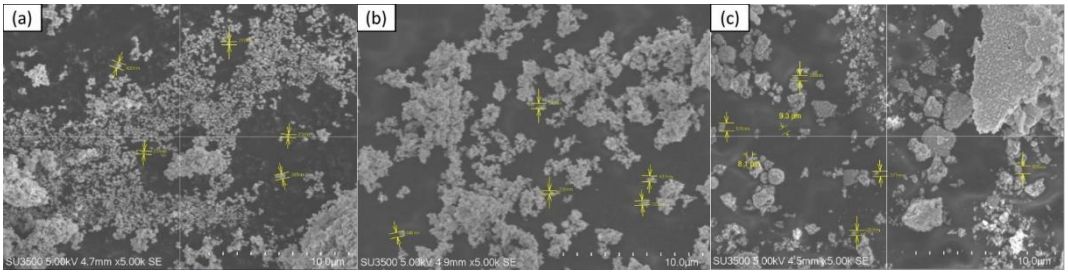

Figure 3 SEM image with of (a) AgNP-Sol, (b) AgNP-Son, and (c) AgNP-Bio.

Furthermore, a qualitative analysis of EDS was carried out to determine the composition of the sample. This analysis is based on X-ray radiation emitted from the atoms in the sample. **Table 4** shows the results of the sample EDS analysis. Based on the results, the largest percentage of Ag atoms was indicated by AgNP-Sol which confirmed the presence of Ag crystal phases other than Ag_2O crystal. In the AgNP-Son result, it was observed that the concentration of Ag was smaller and O was higher than the ratio of the Ag_2O compound. This was associated with O uptake during loading into the microscope. The EDS results can only give approximate compositions, thus the accuracy of EDS results depends on several factors such as matrix, background, peak interference, energy, electron beam quality, and calibration [58]. Then, AgNP-Bio synthesized using biological methods contained other atoms, namely P, N, and S of 13.85, 7.43 and 4.41 %, respectively. It is understood that the biosynthetic method yielded Ag_3PO_4 as shown in the XRD results. In addition, other elements such as N and S derived from the media used can also precipitate.

Table 4 Percentage of atoms in the sample from the EDS analysis.

Sample	Atomic (%)				
	Ag	**O**	**P**	**N**	**S**
AgNP-Sol	64.78	35.22	-	-	-
AgNP-Son	59.22	40.78	-	-	-
AgNP-Bio	33.07	41.24	13.85	7.43	4.41

Particle Size Analysis (PSA)

The particle size distribution of Ag_2O was tested using a particle-size analyzer based on light scattering. **Figure 4** shows that the particle size distribution of Ag_2O is relatively homogeneous, which is characterized by only one peak formed. The results showed that the chemical method (sol-gel and sonochemistry) showed smaller particle sizes than the biological method, with the smallest size being the sol-gel method with a size of 247 nm. This is understandable because the sol-gel method uses PEG surfactant as a capping agent to prevent the agglomeration process [36]. The presence of hydrophobic poles on the capping agent causes the formation of steric barriers that can control particle growth. This reduces the surface energy of the particles, and aggregation can be avoided [59,60]. In the sonochemical method, ultrasonic waves are used to prevent agglomeration resulting in a particle size of 279 nm. Meanwhile, in the biosynthetic method, compounds produced from bacterial metabolism, such as proteins, can also act as natural capping agents [61].

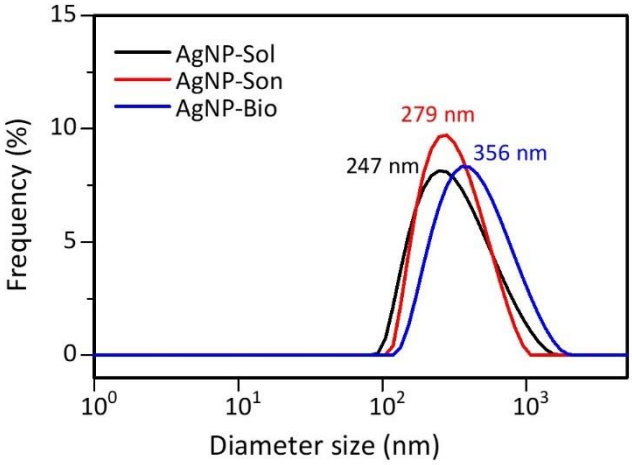

Figure 4 PSA results for Ag_2O particle size distribution.

From the data in **Table 5**, it can be seen that the chemical synthesis method has a smaller z-average or mean particle size than the biological method. In addition, the particle size that occurs the most is observed from the mode value. The mode values of each Ag_2O resulting from sonochemical, sol-gel, and biosynthetic methods were 232.7; 262.1; and 335.7 nm, respectively. The value of the polydispersity index (PI) is a measure of the distribution of the molecular mass in the sample. It is expressed as the average molecular weight of the weight divided by the sum of the average molecular weights [62]. The smallest PI value is in the sonochemical method which indicates that the particle size is evenly distributed and homogeneous. Reducing the size will increase the surface area so as to increase the reactivity as an application in the field of adsorbents [63], catalysts [64], etc.

Table 5 Data measurement results using particle size analyzer.

Sample	Particle size (nm)				
	Mode	**Mean**	**Median**	**Z-average**	**PI**
AgNP-Sol	232.7	340.8	278.7	203.4	0.551
AgNP-Son	262.1	317.4	278.9	237.6	0.469
AgNP-Bio	335.7	462.9	389.0	239.8	0.862

Conclusions

Silver oxide nanoparticles have been successfully synthesized by chemical methods, namely sol-gel and sonochemistry, as well as biological methods. The sol-gel method showed that there were two crystals formed, namely silver and silver oxide with crystallite sizes of 14.6 and 9.5 nm, respectively. The sonochemical method showed that 99.8 % of silver oxide was formed with a crystallite size of 11.1 nm. Meanwhile, an impurity phase was formed from the precursor media, namely Ag_3PO_4 with a crystallite size of 22.2 nm, and the largest crystallite size of Ag_2O is 23.2 nm. From this research, it is also known that the sol-gel method has the largest specific area, which is 60.09 m^2/g compared to the sonochemical and biosynthetic methods, which are 51.78 and 24.77 m^2/g, respectively. From the SEM results, it is known that the chemical method (sol-gel and sonochemistry) has a homogeneous and agglomerated spherical shape, while the biosynthetic method has a flakes-like shape. Silver oxide nanoparticles synthesized using the sol-gel method with PEG surfactant showed the smallest particle size of 232.7 nm, compared to 262.1 nm for the sonochemical method, and 335.7 nm for the biosynthetic method.

Acknowledgements

The authors are grateful for the facilities from Universitas Padjadjaran, Indonesia by Academic Leadership Grant (ALG) Prof. Iman Rahayu (ID: 2203/UN6.3.1/PT.00/2022).

References

[1] KI Kelly, E Coronado, LL Zhao and GC Schatz. The optical properties of metal nanoparticles: The influence of size, shape, and dielectric environment. *J. Phys. Chem. B* 2003; **107**, 668.

[2] H Amrulloh, A Fatiqin, W Simanjuntak, H Afriyani and A Annissa. Bioactivities of nano-scale magnesium oxide prepared using aqueous extract of Moringa oleifera leaves as green agent. *Adv. Nat. Sci. Nanosci. Nanotechnol.* 2021; **12**, 015006.

[3] H Amrulloh, W Simanjuntak, RTM Situmeang, SL Sagala, R Bramawanto, A Fatiqin, R Nahrowi and M Zuniati. Preparation of nano-magnesium oxide from Indonesia local seawater bittern using the electrochemical method. *Inorg. Nano Met. Chem.* 2020; **50**, 693-8.

[4] P Christian, FVD Kammer, M Baalousha and T Hofmann. Nanoparticles: Structure, properties, preparation and behaviour in environmental media. *Ecotoxicology* 2008; **17**, 326.

[5] A Fadaka, O Aluko, S Awawu and K Theledi. Green synthesis of gold nanoparticles using *Pimenta dioica* leaves aqueous extract and their application as photocatalyst, antioxidant, and antibacterial agents. *J. Multidiscip. Appl. Nat. Sci.* 2021; **1**, 78-88.

[6] YF He, DY Chu and Z Zhuo. Cycle stability of dual-phase lithium titanate (LTO)/TiO_2 nanowires as lithium battery anode. *J. Multidiscip. Appl. Nat. Sci.* 2021; **1**, 54-61.

[7] WHD Jong and PJ Borm. Drug delivery and nanoparticles: Applications and hazards. *Int. J. Nanomedicine* 2008; **3**, 133-49.

[8] WJ Stark, PR Stoessel, W. Wohlleben and A Hafner. Industrial applications of nanoparticles. *Chem. Soc. Rev.* 2015; **44**, 5793-805.

[9] I Khan, K Saeed and I Khan. Nanoparticles: Properties, applications and toxicities. *Arabian J. Chem.* 2019; **12**, 908-31.

[10] AJ Varkey and AF Fort. Some optical properties of silver peroxide (AgO) and silver oxide (Ag_2O) films produced by chemical-bath deposition. *Sol. Energ. Mater. Sol. Cell.* 1993; **29**, 253-9.

[11] C Feldmann and C Metzmacher. Polyol mediated synthesis of nanoscale MS particles (M = Zn, Cd, Hg). *J. Mater. Chem.* 2001; **11**, 2603-6.

[12] LM Lyu and MH Huang. Investigation of relative stability of different facets of Ag_2O nanocrystals through face-selective etching. *J. Phys. Chem. C* 2011; **115**, 17768.

[13] L Deleebeeck, D Ippolito and KK Hansen. Enhancing hybrid direct carbon fuel cell anode performance using Ag_2O. *Electrochim. Acta* 2015; **152**, 222-39.

[14] HY Dai, HM Yang, X Jian, X Liu and ZH Liang. Performance of Ag_2O/Ag electrode as cathodic electron acceptor in microbial fuel cell. *Acta. Metall. Sin.* 2017; **30**, 1243-8.

[15] T Ahamad, A Aldalbahi, SM Alshehri, S Alotaibi, S Alzahly, ZB Wang and PX Feng. Enhanced photovoltaic performance of dye-sensitized solar cells based Ag_2O doped $BiFeO_3$ hetrostructures. *Sol. Energ.* 2021; **220**, 758-65.

[16] X Wang, S Li, H Yu, J Yu and S Liu. Ag_2O as a new visible-light photocatalyst: self-stability and high photocatalytic activity. *Chemistry* 2011; **17**, 7777-80.

[17] Y Wang, N Bi, H Zhang, W Tian, T Zhang, P Wu and W Jiang. Visible-light-driven photocatalysis-assisted adsorption of azo dyes using Ag_2O. *Colloid. Surface. Physicochem. Eng. Aspect.* 2020; **585**, 124105.

[18] Y Volokitin, JD Sinzig, LJD Jongh, G Schmid, MN Vargaftik and II Moiseevi. Quantum-size effects in the thermodynamic properties of metallic nanoparticles. *Nature* 1996; **384**, 621-3.

[19] K Kayed. The optical properties of individual silver nanoparticles in Ag/Ag_2O composites synthesized by oxygen plasma treatment of silver thin films. *Plasmonics* 2020; **15**, 1439-49.

[20] LCAD Silva, FG Neto, SSC Pimentel, PRD Silva, F Sato, KM Retamiro, NS Fernandes, CV Nakamura, F Pedrochi and A Steimacher. The role of Ag_2O on antibacterial and bioactive properties of borate glasses. *J. Non Crystalline Sol.* 2021; **554**, 120611.

[21] A Kumar, MK Bhatt, SK Singh, SK Singh, RJ Bhatt and NA Karimi. Synthesis and characterization of silver oxide and silver nanoparticle by sol-gel method. *Bull. Pure Appl. Sci. Chem.* 2010; **29**, 101-8.

[22] S Sagadevan. Synthesis, structural, surface morphology, optical and electrical properties of silver oxide nanoparticles. *Int. J. Nanoelectron. Mater.* 2016; **9**, 37-49.

[23] YP Zhu, XK Wang, WL Guo, JG Wang and C Wang. Sonochemical synthesis of silver nanorods by reduction of sliver nitrate in aqueous solution. *Ultrason. Sonochem.* 2010; **17**, 675-9.
[24] IA Wani, A Ganguly, J Ahmed and T Ahmad. Silver nanoparticles: Ultrasonic wave assisted synthesis, optical characterization and surface area studies. *Mater. Lett*. 2011; **65**, 520-2.
[25] Y Li, P Ren, W Wu, C Chen and M Wu. Solvothermal synthesis and electrochemical properties of octahedral cobalt oxide decorated with Ag_2O. *J. Wuhan Univ. Tech. Mater. Sci. Ed.* 2017; **32**, 568-73.
[26] A Zielińska-Jurek, J Reszczyńska, E Grabowska and A Zaleska. *Nanoparticles preparation using microemulsion systems*. *In*: R Najjar (Ed.). Microemulsions-an introduction to properties and applications. IntechOpen, London, 2021, p. 229-50.
[27] IA Wani, S Khatoon, A Ganguly, J Ahmed and T Ahmad. Structural characterization and antimicrobial properties of silver nanoparticles prepared by inverse microemulsion method. *Colloid. Surface. B Biointerfaces* 2013; **101**, 243-50.
[28] SR Shaffiey, SF Shaffiey and M Ahmadi. Synthesis and evaluation of bactericidal properties of Ag_2O nanoparticles against *Aeromonas hydrophila*. *Int. J. Nano Dimension* 2015; **6**, 263-9.
[29] NS Flores-Lopez, JA Cervantes-Chávez, DG Téllez de Jesús, M Cortez-Valadez, M Estévez-González and R Esparza. Bactericidal and fungicidal capacity of Ag_2O/Ag nanoparticles synthesized with *Aloe vera* extract. *J. Environ. Sci. Health* 2021; **56**, 762-8.
[30] S Iravani. Green synthesis of metal nanoparticles using plants. *Green Chem.* 2011; **13**, 2638-50.
[31] H Korbekandi, S Iravani and S Abbasi. Production of nanoparticles using organisms. *Crit. Rev. Biotechnol*. 2009; **29**, 279-306.
[32] HJ Jeon, SC Yi and SG Oh. Preparation and antibacterial effects of Ag-SiO_2 thin films by sol-gel method. *Biomaterials* 2003; **24**, 4921-8.
[33] XK Wang, L Shao, WL Guo, JG Wang, YP Zhu and C Wang. Synthesis of dendritic silver nanostructures by means of ultrasonic irradiation. *Ultrason. Sonochem.* 2009; **16**, 747-51.
[34] J Zhu, X Liao and HY Chen. Electrochemical preparation of silver dendrites in the presence of DNA. *Mater. Res. Bull.* 2001; **36**, 1687-92.
[35] ZH Dhoondia and H Chakraborty. Lactobacillus mediated synthesis of silver oxide nanoparticles. *Nanomater. Nanotechnol*. 2012; **2**, 55741.
[36] NL Yong, A Ahmad and AW Mohammad. Synthesis and characterization of silver oxide nanoparticles by a novel method. *Int. J. Sci. Eng. Res.* 2013; **4**, 155.
[37] T Ahmad, IA Wani, OA Al-Hartomy, AS Al-Shihri and A Kalam. Low temperature chemical synthesis and comparative studies of silver oxide nanoparticles. *J. Mol. Struct.* 2015; **1084**, 9-15.
[38] P Norby, R Dinnebier and AN Fitch. Decomposition of silver carbonate; the crystal structure of two high-temperature modifications of Ag_2CO_3. *Inorg. Chem.* 2002; **41**, 3628-37.
[39] XS Yan, P Lin, X Qi and L Yang. Finnis-Sinclair potentials for fcc Au-Pd and Ag-Pt alloys. *Int. J. Mater. Res.* 2011; **102**, 381.
[40] MN Deschizeaux-Cheruy, JJ Aubert, JC Joubert, JJ Capponi and H Vincent. Relation entre structure et conductivite ionique basse temperature de Ag_3PO_4. *Solid State Ionics* 1982; **7**, 171-6.
[41] K Shameli, M Bin Ahmad, SD Jazayeri, S Sedaghat, P Shabanzadeh, H Jahangirian, M Mahdavi and Y Abdollahi. Synthesis and characterization of polyethylene glycol mediated silver nanoparticles by the green method. *Int. J. Mol. Sci*. 2012; **13**, 6639-50.
[42] P Simakova, J Gautier, M Prochazka, K Herve-Aubert and I Chourpa. Polyethylene-glycol-stabilized Ag nanoparticles for surface-enhanced raman scattering spectroscopy: Ag surface accessibility studied using metalation of free-base porphyrins. *J. Phys. Chem. C* 2014; **118**, 7690-7.
[43] T Degen, M Sadki, E Bron, U König and G Nénert. The highscore suite. *Powder Diffract.* 2014; **29**, S13-8.
[44] SP Yadav, SS Shinde, P Bhatt, SS Meena and KY Rajpure. Distribution of cations in $Co_{1-x}Mn_xFe_2O_4$ using XRD, magnetization and Mössbauer spectroscopy. *J. Alloy. Comp.* 2015; **646**, 550-6.
[45] A Luthfiah, MD Permana, Y Deawati, ML Firdaus, I Rahayu and DR Eddy. Photocatalysis of nanocomposite titania-natural silica as antibacterial against *Staphylococcus aureus* and *Pseudomonas aeruginosa*. *RSC Adv.* 2021; **11**, 38528.
[46] JI Langford and AJC Wilson. Scherrer after sixty years: A survey and some new results in the determination of crystallite size. *J. Appl. Crystallogr.* 1978; **11**, 102-13.
[47] M Dhaouadi, M Jlassi, I Sta, IB Miled, G Mousdis, M Kompitsas and W Dimassi. Physical properties of copper oxide thin films prepared by sol-gel spin-coating method. *Am. J. Phys. Appl*. 2018; **6**, 43-50.

[48] L Abbasi, K Hedayati and D Ghanbari. Magnetic properties and kinetic roughening study of prepared polyaniline: Lead ferrite, cobalt ferrite and nickel ferrite nanocomposites electrodeposited thin films. *J. Mater. Sci. Mater. Electron.* 2021; **32**, 14477-93.
[49] P Dhatarwal and RJ Sengwa. Polymer compositional ratio-dependent morphology, crystallinity, dielectric dispersion, structural dynamics, and electrical conductivity of PVDF/PEO blend films. *Macromol. Res.* 2019; **27**, 1009-23.
[50] M Bellardita, AD Paola, B Megna and L Palmisano. Determination of the crystallinity of TiO_2 photocatalysts. *J. Photochem. Photobiol. Chem.* 2018; **367**, 312-20.
[51] J Sun, Z Zhang, J Ji, M Dou and F Wang. Removal of Cr^{6+} from wastewater via adsorption with high-specific-surface-area nitrogen-doped hierarchical porous carbon derived from silkworm cocoon. *Appl. Surf. Sci.* 2017; **405**, 372-9.
[52] X Zhang, F Hou, H Li, Y Yang, Y Wang, N Liu and Y Yang. A strawsheave-like metal organic framework Ce-BTC derivative containing high specific surface area for improving the catalytic activity of CO oxidation reaction. *Microporous Mesoporous Mater.* 2018; **259**, 211-19.
[53] P Bernard, P Stelmachowski, P Broś, W Makowski and A Kotarba. Demonstration of the influence of specific surface area on reaction rate in heterogeneous catalysis. *J. Chem. Educ.* 2021; **98**, 935-40.
[54] MP Gómez-Tena, J Gilabert, J Toledo, E Zumaquero and C Machí. Relationship between the specific surface area parameters determined using different analytical techniques. *In*: Proceedings of the XII Foro Global Del Recubrimiento Cerámico, Castellón, Spain. 2014.
[55] M Shahjahan, MH Rahman, MS Hossain, MA Khatun, A Islam and MHA Begum. Synthesis and characterization of silver nanoparticles by sol-gel technique. *Nanosci. Nanometrol.* 2017; **3**, 34-39.
[56] HV Swygenhoven. Grain boundaries and dislocations. *Science* 2002; **296**, 66-7.
[57] GZ Voyiadjis and FH Abed. Effect of dislocation density evolution on the thermomechanical response of metals with different crystal structures at low and high strain rates and temperatures. *Arch. Mech.* 2005; **57**, 299-343.
[58] KG Raghavendra, A Dasgupta, P Bhaskar, K Jayasankar, CN Athreya, P Panda, S Saroja, VS Sarma and R Ramaseshan. Synthesis and characterization of Fe-15 wt.% ZrO2 nanocomposite powders by mechanical milling. *Powder Tech.* 2016; **287**, 190-200.
[59] CM Phan and HM Nguyen. Role of capping agent in wet synthesis of nanoparticles. *J. Phys. Chem. A* 2017; **121**, 3213-9.
[60] DR Eddy, D Nursyamsiah, MD Permana, AR Noviyanti and I Rahayu. Green production of zero-valent iron (ZVI) using tea-leaf extracts for fenton degradation of mixed rhodamine B and methyl orange dyes. *Materials* 2022; **15**, 332.
[61] F Mulyani, MD Permana, S Ishmayana, I Rahayu and DR Eddy. Optimisation of zinc oxide nanoparticle biosynthesis using *Saccharomyces Cerevisiae* with box-behnken design. *Rev. Chem.* 2021; **72**, 78-89.
[62] DR Eddy, SN Ishmah, MD Permana, ML Firdaus, I Rahayu, YA El-Badry, EE Hussein and ZM El-Bahy. Photocatalytic phenol degradation by silica-modified titanium dioxide. *Appl. Sci.* 2021; **11**, 9033.
[63] J Choi, A Ide, YB Truong, IL Kyratzis and RA Caruso. High surface area mesoporous titanium-zirconium oxide nanofibrous web: A heavy metal ion adsorbent. *J. Mater. Chem. A* 2013; **1**, 5847-53.
[64] R Moene, M Makkee and JA Moulijn. High surface area silicon carbide as catalyst support characterization and stability. *Appl. Catal. Gen.* 1998; **167**, 321-30.